In-orbit Interference Measurements and Analysis in the VDES-band with the NorSat-2 Satellite

Gara Quintana-Diaz
Department of Electronic Systems
Norwegian University of Science and Technology (NTNU)
7491 Trondheim, Norway
gara.quintana@ntnu.no

Roger Birkeland
Department of Electronic Systems
NTNU
7491 Trondheim, Norway
roger.birkeland@ntnu.no

Lars Løge
Space Norway AS
0212 Oslo, Norway
lars.loge@spacenorway.no

Even Andersen
Space Norway AS
0212 Oslo, Norway
even.sogn.andersen@spacenorway.no

Anton Bolstad
Space Norway AS
0212 Oslo, Norway
anton.bolstad@spacenorway.no

Torbjörn Ekman
Department of Electronic Systems
NTNU
7491 Trondheim, Norway
torbjorn.ekman@ntnu.no

Abstract—Maritime activity in the Arctic is increasing, triggering a need for better communication infrastructure. With limited terrestrial infrastructure available, satellite services are essential for distributing maritime safety information, such as ice and weather information, navigational augmentation data, and basic communication to vessels operating in the vulnerable Arctic environment. The VHF Data Exchange System (VDES) is a new communication system for ships, extending the successful Automatic Identification System (AIS). VDES has a satellite component (VDE-SAT) which will extend the terrestrial-based coastal coverage to global coverage. Measurements and analysis of the in-orbit radio environment are needed to improve the robustness and reliability of the VDE-SAT system. Knowledge and understanding of the in-orbit interference will allow the development of appropriate interference mitigation techniques. This paper presents preliminary in-orbit measurement results and analysis of the radio environment in the VDE-SAT frequencies in the 157.2875 – 157.3375 MHz band. The measurements were carried out using the VDE-SAT payload on-board the Norwegian NorSat-2 satellite. We analyze the time-frequency characteristics of interference by studying two types of statistics on the raw in-phase and quadrature samples: the general temporal dynamic of the interference, characterised using the Local Mean Envelope (LME) for different averaging window lengths; and the interference duration and periodicity. Both these views play a role when choosing suitable countermeasures to get robust communications. The coefficient of variation on the LME is used to study the dispersion. Data from two measurement campaigns over the Arctic area from May 2021 are analysed using these two methods, and the initial results are presented.

TABLE OF CONTENTS

1. INTRODUCTION

Global warming is affecting the Arctic and the temperature is rising at even higher rates than the rest of the world [1]. The ice is melting and some predictions indicate there could be ice-free summers in this century [2]. Ship traffic routes will constantly change due to ice melting, and navigation of these areas will be difficult without frequently updated ice charts. Thus, increased connectivity and reliable communication to ships in the Arctic is needed [3], and terrestrial communication is seldom available. Therefore, satellite services will play a key role in this scenario, as they provide digital communication to vessels far from coastal infrastructure.

The Automatic Identification System (AIS) is a maritime communication system used for ship safety and navigation aid [4] that also has a satellite component to increase coverage. The main focus of the AIS is to avoid vessel collisions by broadcasting the position, speed, and course of all ships above a given size. All nearby ships can then follow the navigational status of the transmitter on their navigation system. Furthermore, AIS data can be used for different purposes, like search-and-rescue operations [5], as well as estimating sea pollution from ships [6], fighting illegal fishing, among many others. However, the success of the AIS system resulted in a huge increase of users, overloading the system in areas with high maritime traffic [7]. Thus, the International Association of Lighthouse Authorities (IALA) and its members started developing the VHF Data Exchange System (VDES) to offload the data traffic of the AIS and to provide new capabilities, such as ship-to-ship messaging [8] and distribution of ice charts to aid navigation [9]. The VDES standard was approved in 2015 and is formed by three services: AIS, Application Specific Messages (ASM) and VHF Data Exchange (VDE) [10], [11]. The ASM channels are used to send predefined messages to report weather conditions, safety and navigational purposes [12]. VDE is more flexible and has a terrestrial component (VDE-TER) and a satellite component (VDE-SAT). Both VDE types, as well as ASM, support Adaptive Coding and Modulation (ACM), allowing for changing modulation and error correction codes while adapting to varying communication conditions.

Choosing the right modulation and error coding is vital to increase the data throughput effectively. This selection depends on channel and interference behaviour in the fre-

quency band used. For the VHF maritime propagation channel, there have been some studies on the empirical path loss [13], [14] and signal propagation at sea [15]. A channel model for VDE-SAT is presented in [16]. The first VDE-SAT downlink measurements were performed in November 2017 using the NorSat-2 satellite [17]. Three different types of VDES signals, in addition to a Continuous Wave (CW), were transmitted from the satellite: Binary Phase Shift Keying (BPSK)/Code Division Multiple Access (CDMA), $\pi/4$-Quadrature Phase Shift Keying (QPSK) and 8-Phase Shift Keying (PSK). The signals were received on two vessels and raw In-Phase Quadrature (IQ) samples were recorded. Initial analysis of the variation of the carrier-to-noise-density ratio (C/N_o) for each signal type over a pass was carried out in [17]. In [9], the variation of the downlinked CW signal power and Doppler shift was analysed for more than a 100 passes. The typical carrier received power on-board a vessel was -118 dBm for the measurements performed. Further analysis on the beacon power distribution and fading distribution estimations can be found in [18]. However, all these VDE-SAT measurement results have focused on the downlink performance. The interference environment encountered when satellites receive messages from vessels is still not characterised. This is needed to establish a reliable two-way communication.

In this paper, we present a preliminary analysis of the time-frequency characteristics of the radio interference in the lower leg of the uplink VDE-SAT frequency band (157.2875 – 157.3375 MHz) over the Arctic area. Two measurement campaigns on two consecutive days were performed with the NorSat-2 satellite, where IQ samples were recorded for post-processing using the Local Mean Envelope (LME) method and a pulse detection algorithm. The results of this project can be used to plan future measurements with NorSat-2 or other satellites. Measurement results can be used to optimise waveforms in the VDES standard.

The remainder of the manuscript is structured as follows. First, the NorSat-2 satellite and the analysis method are described, as well as the measurement planning and configuration. Second, the results of the measurement campaigns are presented. Finally, the conclusions are presented.

2. METHOD

In this section, the measurement strategy, and the analysis methods are explained. Two algorithms to measure time and frequency characteristics of interference are described.

The NorSat-2 satellite

NorSat-2 was launched in July 2017, and was built by University of Toronto Institute for Aerospace Studies (UTIAS) for the Norwegian Space Agency (NOSA) [19]. It has two main objectives: primarily, to collect AIS data from ships and forward it to Norwegian users, mainly the Norwegian Coastal Administration (NCA). Secondary, to demonstrate the use of the VDE-SAT with a VDE-SAT payload owned by Space Norway, and developed by Kongsberg Seatex. The VDE-SAT payload is based on Software-Defined Radio (SDR) technology and is connected to a folded dipole Yagi-Uda VHF antenna with three cross elements providing 8 dBi gain.

The SDR payload can also be used to measure the in-orbit radio environment in the VDES bands by storing the raw IQ samples recorded. To measure the radio environment, the satellite will be listening without transmitting. The

samples will be downloaded and processed on ground with different algorithms to, for example, detect and characterize any measured interference. In the next section, two different algorithms to analyse interference will be presented.

Local Mean Envelope (LME)

The LME method is a low-complexity algorithm that measures both time and frequency characteristics of a signal [20]. Firstly, Discrete Fourier Transforms (DFTs) of the incoming IQ data are calculated throughout the measurement duration. Secondly, the mean of the envelope for each frequency bin is estimated throughout all the measurement duration, as well as the average power in the same time frame. The time variability comes from estimating the local mean envelopes for different time window lengths for each frequency bin. The coefficient of variation (CV) is used to calculate the dispersion of the data and the first-order stationarity window.

Detection of pulsed interference

A simple algorithm to automatically detect pulsed interference and their characteristics (pulse length and pulse period) was implemented. The absolute value of the complex signal formed by the raw IQ samples recorded is calculated and a median filter is applied to smooth out the signal. After smoothing the signal, signal pulses can be detected. The minimum detectable pulse length is approximately 7 μs and the minimum detectable pulse period was 0.7 ms due to the configuration of the algorithm. The edges of the pulses yield the pulse length, and its period is estimated as the difference of the position where the pulses were detected.

Measurement planning

The main target of interest is the Arctic Ocean, where VDE-SAT can be used to distribute ice charts and help increase maritime safety. Ten different measurement tracks centered at Bjørnøya/Bear Island (Norway) were recorded in May 2021. The raw IQ data captured by the SDR onboard NorSat-2 was saved for post-processing on ground. Each track is referred to as *one session* and lasted approximately 10-12 minutes. Five sessions were recorded on the 5th of May (S13-S17) and the next five sessions were executed the next day at similar times (S18-S22) so that the tracks were close to each other, see Figure 1.

Measurement configuration

The measurement configuration used in these campaigns is summarised in Table 1. The center frequency chosen was the nominal uplink frequency for VDE-SAT in the lower leg to measure the interference received by the satellite, and the bandwidth corresponds to the channel bandwidth of VDE-SAT [8]. The Automatic Gain Control (AGC) was deactivated to keep the same gain for all measurement points. All power values relate to the output of the VHF antenna. The satellite was configured to point the satellite antenna towards the horizon in the direction of Bjørnøya (Norway) in all passes, so the antenna was tracking that target for the measurements. The measurements were carried out without the satellite transmitting any signal to be able to measure the noise and interference environment.

3. MEASUREMENT RESULTS

To get an overview of the measured power (interference) in the different sessions, the Empirical Cumulative Density Function (ECDF) of instantaneous power received for each
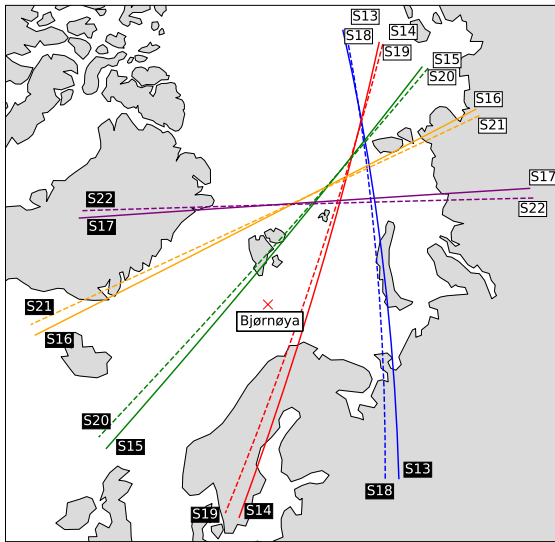
2

Figure 1: **Measurement tracks. Tracks S13-S17 were recorded on 5th May 2021 and S18-S22 on 6th May 2021. White squares indicate where the satellite started the track and black squares where it ended.**

Figure 2: **Empirical Cumulative Density Function (ECDF) of instantaneous power received over the tracks. Same colour indicate similar tracks performed in two consecutive days. The tracks of the first day are in continuous lines and the second day, in dashed lines.**

Table 1: **Measurement configuration**

Parameter	Value
Center frequency (MHz)	157.3125
Bandwidth (kHz)	50
Sampling rate (kSps)	134.4
Number of bits per sample	8

session is calculated using the raw IQ samples (Figure 2). The sessions that follow similar tracks in the two consecutive days, are plotted with the same colour. Continuous lines indicate sessions taken the 5th May and dashed lines, 6th May. It can be seen that lines with the same colour have very similar power distributions, which means that the distribution of instantaneous power over those locations did not change considerably from the first measurement day to the second. The tracks *S13* and *S18* show slightly less power than the rest. However, all measured tracks have a similar distribution of instantaneous power. These measurements give an indication of the power distribution, but more measurements are necessary to address time variability over larger time scales. The steps that appear in the ECDFs are due to the 8 bit quantization. Most of the power values lie on the lowest bits.

The percentiles of average power spectrum density during one-second segments of all measurement sessions are shown in Figure 3. The drop in power at 157.2875 and 157.3375 MHz coincides with the 50 kHz bandwidth configured. However, this drop is much bigger for the 10% percentile spectrum (15 dB) than for the 50% (median) or 90% percentile, 5 and 3 dB. There is a big dispersion in the spectra. Within the configured bandwidth, there is about 15 dB less power density in the 10% percentile compared to the median, and 4 dB less from the median to the 90% percentile. Thus, 50% of the power spectral density averages are above -142 dBm/Hz in the considered bandwidth. Furthermore, there is a narrow-band signal in the center of the band.
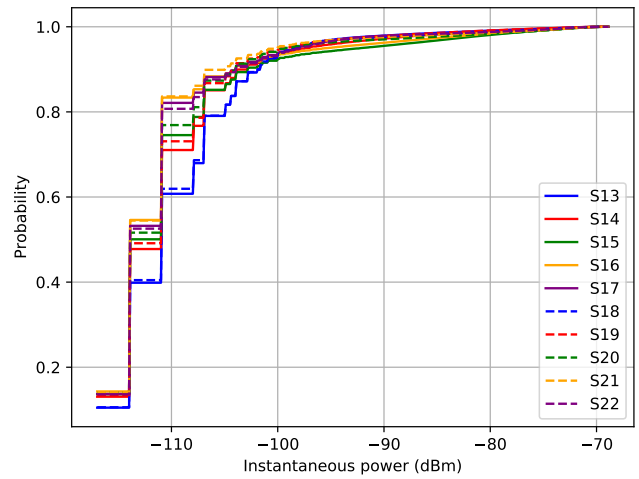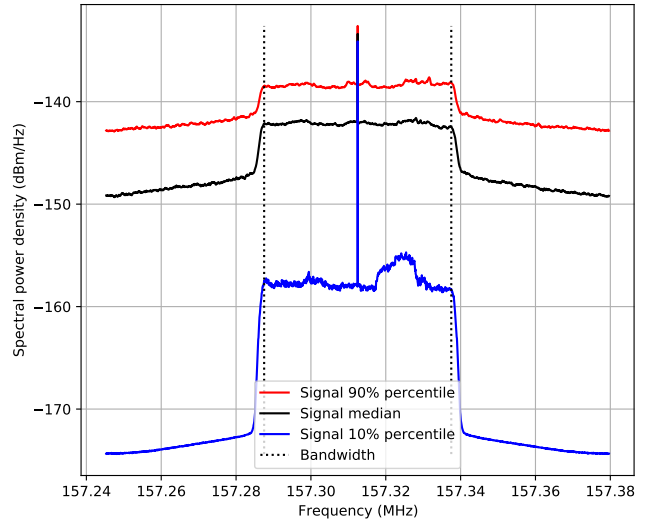

Figure 3: **Average power spectral density percentiles.**

The coefficient of variation c_k was calculated to analyse the dispersion of the data and compare it with the CV of Additive White Gaussian Noise (AWGN). As it can be seen in Figure 4, there are different frequency behaviours. The narrow-band signal has a CV close to zero, indicating low dispersion in the envelope. Since the signal is narrow-band, does not vary in time, and is in the center of the band, it is most likely the local oscillator of the receiver. For the 10% percentile, the CV out of band is the same as the one for AWGN, and within the bandwidth, the CV is slightly higher. However, for the median and 90% percentile, the CV out of band is higher than the one in-band. The CV in-band is also much higher than for the 10% percentile, indicating that the measured interference is be pulsed. The signals out of band are more attenuated than the one in-band due to the 50 kHz digital filter, and they have a larger dispersion. The difference between Figure 4a and Figure 4b is that the first one uses segments of 2048 samples to calculate the DFT, which is equivalent to 15 ms of signal;

3

and the second one uses segments of 32 samples (0.24 ms). Hence, in Figure 4a the variability within 15 ms cannot be appreciated in the CV, whereas in Figure 4b the CV is higher, indicating that there was a high variability within 15 ms.
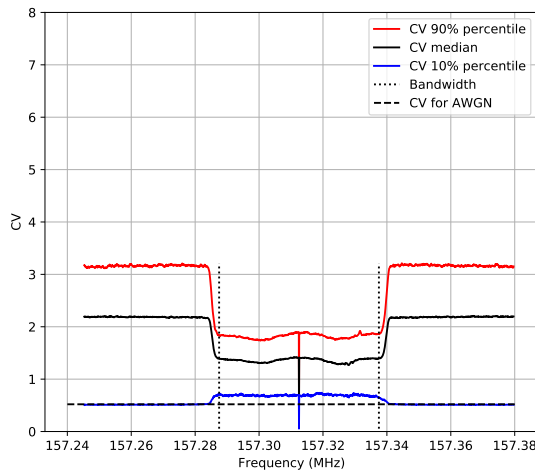
(a) **CV calculated from DFT segments of 2048 frequency bins (15 ms).**
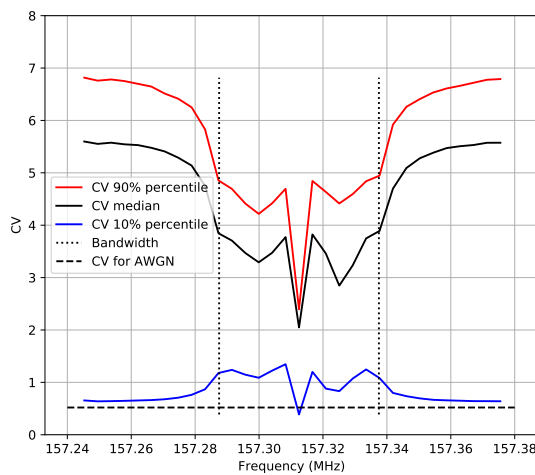
(b) **CV calculated from DFT segments of 32 frequency bins (0.2 ms).**

Figure 4: **CV. A high CV indicates high spread in the measured envelope.**

In satellite communications, time variability on the order of seconds implies spatial variability since the satellite is orbiting the Earth. In Figure 5a, the tracks have been divided into four regions according to the average local power while avoiding rapid changes between region: $R1$ from -100 dBm to -95 dBm, $R2$ from -95 dBm to -90 dBm, $R3$ from -110 dBm to -100 dBm, and $R4$ from -115 dBm to -110 dBm. The power is the sum of the average power in the frequency bins within the bandwidth. The ECDFs of this power measure over the regions are presented in Figure 5b. The red curve represents the ECDF of the power of all regions. Region $R2$ (black), where all tracks crossed each other, shows the highest interference in the measurements. The ECDF of the region $R1$ (yellow) shows less power than region $R2$, but higher than the two other regions, and it does not appear in all tracks. Region $R3$ shows less power than the previous regions

and is present in the second part of the tracks. Finally, the magenta region appears at the beginning of tracks $S13$/$S18$ and $S14$/$S19$, and at the end of $S16$/$S21$ and $S17$/$S22$. This region receives very little power.
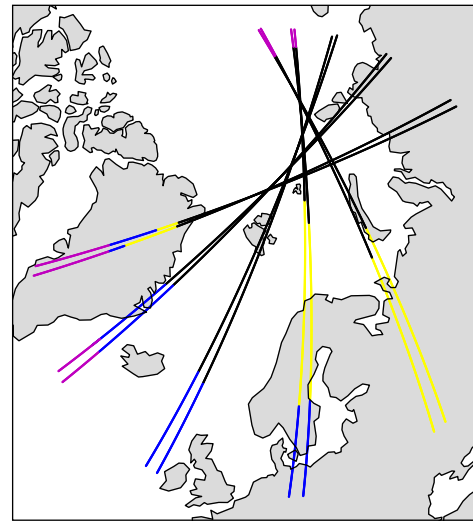
(a) **Sub-satellite points grouped into four regions chosen based on the average local power.**
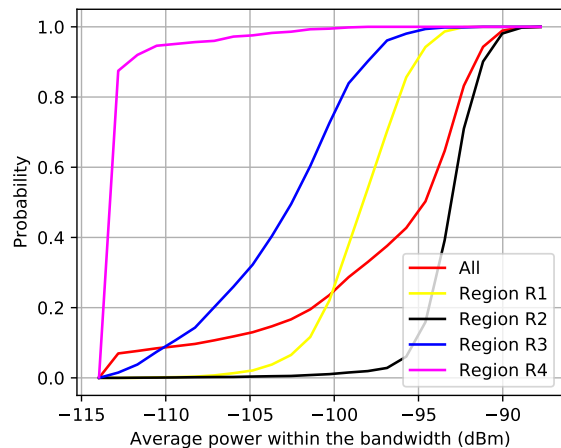

(b) **ECDF of average power within the bandwidth.**

Figure 5: **Power distribution of measurement tracks divided into four regions.**

Using the LME method and the CV, the window of stationarity has been calculated for each region (Figure 6). In this paper, we define first-order stationarity as when the coefficient of variation of the local means is below -10 dB as in [20]. When the CV of the local mean of a specific window reaches this convergence, that window is referred to as the stationarity window. The shortest window for region $R1$ is 0.95 ms, for a tiny percentage of points. The percentage slowly increases when the windows are larger, but almost 55% of the points have a window of stationarity longer than 121.9 ms. This means that there is high variability between long local means of the signal envelope and that the one-second measurement has non-stationary statistics. Region $R2$ has even a larger percentage of points (around 76 %) with a stationarity window longer than 121.9 ms. This percentage of points for windows smaller than 61 ms is very low, increasing

4

to 7.5% for 61 ms and 16% for 121.9 ms. Region $R3$ has a slightly higher percentage of points in shorter windows, as compared to region $R2$, having almost 39% of the points with a stationarity window longer than 121.9 ms. The trend changes in the region $R4$ where about 67% of the points have a stationarity window close to 0.95 ms, and the rest have different windows. It seems that a time window of 0.95 ms is long enough to have similar statistics and be stationary in this region.
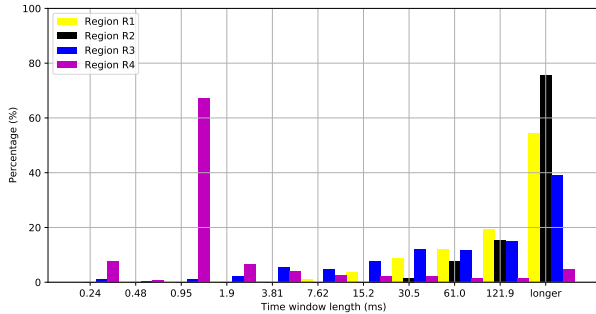
**Figure 6**: **Histogram of stationarity window per region (within the bandwidth).**

Visual analysis confirms that the interference detected has a pulsed structure. In Figure 7, a segment of the in-phase signal captured in track $S13$ at different time scales is shown as an example of the interference encountered. In the largest time scale, several interference pulses of different amplitudes can be seen. When zooming in on that time scale, the pulse structure is recognised. Different pulses can be seen with different pulse periods. In the smallest time scale, zooming in on a typical 1.6 ms pulse, the time structure of the pulse can be seen and the amplitude varies within the pulse length.
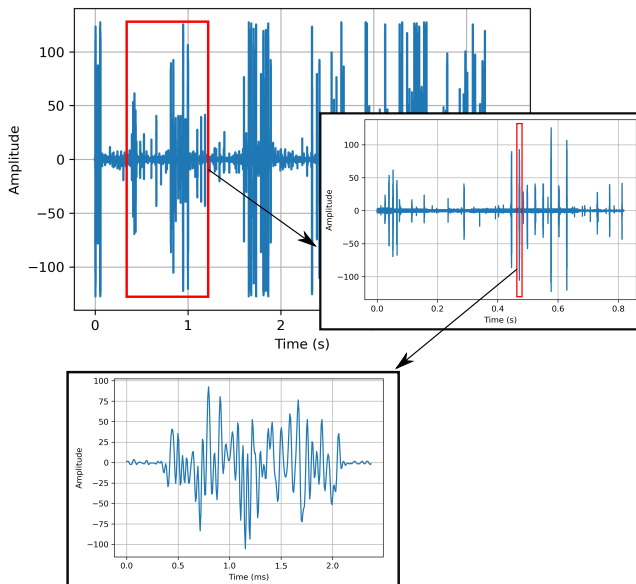
**Figure 7**: **In-phase signal at different time scales.**

An algorithm to detect pulses was applied to the time data of each session, as explained in section 2, to gather statistics of interference characteristics. An algorithm to detect pulse lengths and pulse periods was applied to the IQ data of each session, as explained in section 2, to gather statistics of interference characteristics. In Figure 8, the pulse length (red

dots) and its corresponding period with respect to the next pulse (blue dots) in track $S13$ are plotted against the number of pulses detected in the session. In the large time scale picture, a cloud of pulse periods ranging from almost zero to 1700 ms can be seen, whereas the pulse length dots are all aligned throughout the track. The longest pulse periods can be neglected in this analysis, since the detection algorithm would detect long periods if after a pulse train the next pulse train is far away, due to the differentiation of position explained in section 2. If the time axis is zoomed in, the pulse characteristics are shown more clearly. This segment corresponds to the same segment shown in the second zoom-in picture of Figure 7. The pulse length is still a continuous row of dots with a value of approximately 1.6 ms. However, the pulse period varies even in a short time scale, changing from 26 ms to 13 ms and 52 ms in this particular example.
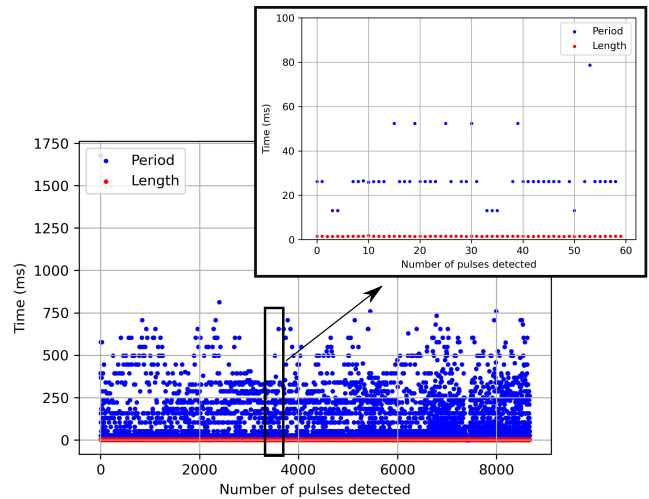
**Figure 8**: **Pulse period pattern at different time scales.**

To verify that the pulse period is consistent throughout all the measurements, the distribution of the pulse length of detected pulses in each region is depicted in Figure 9. All regions have a similar distribution, where almost all pulses have a length of approximately 1.6 ms, within the studied bandwidth. Regions $R1$ and $R2$ have a small percentage of pulses with a shorter length.
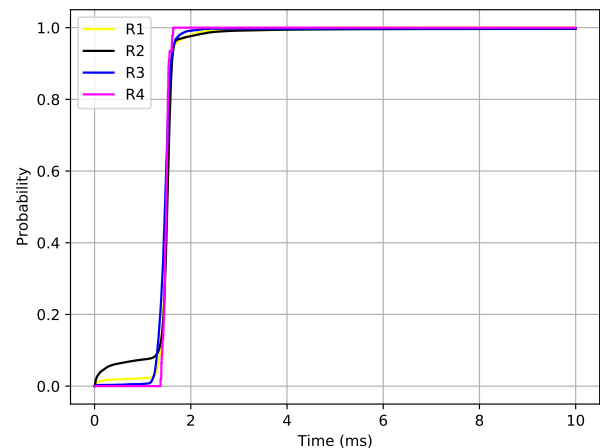
Figure 9: **ECDF of pulse length detected in the different regions.**

5

The ECDF of the pulse period estimated for detected pulses in the different regions is depicted in Figure 10. In region $R4$, 48% of the pulses detected have a period lower than 53 ms, and in the region $R3$, 56%. The percentages for regions $R2$ and $R1$ are 81% and 72%. In $R4$, lower signal power was detected which would mean a lower signal-to-noise ratio (the pulses being the signal in this case). Hence, it is reasonable that the detected pulse period is longer as some pulses are missed. In general, the most common periods are 13 ms (3% in $R3$ and $R4$, 12% in $R1$ and 14% in $R2$), 26 ms (34% in $R4$, 11% in $R3$, 42% in $R1$ and 59% in $R2$), 41 ms and 52 ms, which would mean a duty cycle of 12.3%, 6%, 3.8% and 3% with the pulse length of 1.6 ms. The pulse period changes throughout the measurement with a train of pulses of one period and then another train of a different number of pulses of a different period as shown in Figure 8, but no clear pattern has been detected.
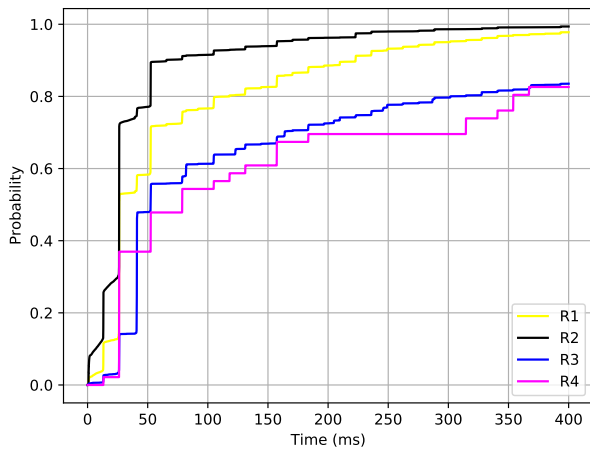
Figure 10: **ECDF of pulse period detected in the different region.**

4. DISCUSSION

When uplinking information in the VDE-SAT band, the detected pulses will interfere with the signal. Instantaneous interference power of up to -70 dBm has been detected, but it could have been higher. The configuration limited the maximum power that could be measured. Observed VDE-SAT signal power from previous experiments was between -90 and -110 dBm. Hence, the interference is between 20 and 40 dB above the desired signal. CDMA has been successfully applied as a mitigation, but other possible countermeasures could be applied. The worst-case is when the pulses have a period of 13 ms. If the transmitted packet length was 13 ms, the pulses were 1.6 ms long and the period between pulses was 13 ms, 12% of the packet would be lost to interference. Error-correcting codes must then account for losing this 12% of data. In addition, the header needs to be protected against these errors. An interleaver with a depth that matches or exceeds the pulse length can be used to spread out the burst errors in different parts of the packet. Furthermore, the communication system could be improved from a worst-case design by changing parameters (modulation, coding and waveform) depending on the region.

In this paper we provided a preliminary time-frequency analysis of the in-orbit interference measured in a small area of the Arctic, but more measurements are needed to obtain reliable interference statistics both at different time scales and larger areas. Furthermore, the data used had only 8 bits which reduces the resolution. Interference power could be higher than reported here, so measurements with more bits and different dynamic ranges would be desired.

A long measurement campaign would enable the first step of increasing the data throughout by selecting different communication parameters and improving the waveforms in the standard depending on which area the satellite is over. ACM can be challenging due to fast variations of the uplink interference, as seen in this article. However, it can be tested in the future.

5. CONCLUSION

In this article, we presented the results of a preliminary measurement campaign of in-orbit interference in the lower leg of the VDE-SAT frequency band (157.2875-157.3375 MHz) using the NorSat-2 satellite. Raw IQ data was captured for ten satellite passes in May 2021 over the Arctic area around Bjørnøya/Bear Island (Norway). The data was processed using the LME method to analyze its time and frequency variability, and an algorithm for pulse detection to characterize interference characteristics.

High levels of pulsed interference covering the full measured bandwidth were detected in the measurement area with instantaneous uplink interference power up to -70 dBm, which is 20 to 40 dB above the uplink signal power. The power can be even higher but due to the small dynamic range in the measurements, the maximum power measured is limited by the measurement configuration. Detected interference varied both within a short time scale and within different regions. The statistics of the interference were highly variable even within one second. The window of stationarity of first-order of the data was estimated for different regions. Most of the measured points have a stationarity window longer than 121.9 ms for most regions, but for the region that received the least interference power, the window is 0.95 ms for 67% of the points. The main measured interference source is pulsed and has a pulse length of about 1.6 ms and the most common pulse periods detected were 13, 26, 41 and 52 ms.

From the measurements analyzed in this paper, it seems that the VDE-SAT communication system should be configured either for the worst-case over a larger area or be adaptive within smaller areas to maximise data throughput. The first step would be to fix communication parameters in different regions. As an example, the pulse length can be used as the minimum depth of an interleaver to spread out errors in the frame and enable error correction after burst events. However, more measurements are necessary to provide more reliable statistics over larger areas and longer time.

REFERENCES

[1] V. A. Semenov, "Modern Arctic Climate Research: Progress, Change of Concepts, and Urgent Problems," *Izvestiya, Atmospheric and Oceanic Physics*, vol. 57, no. 1, pp. 18–28, 2021. [Online]. Available: https://doi.org/10.1134/S0001433821010114

[2] N. Wunderling, M. Willeit, J. F. Donges, and R. Winkelmann, "Global warming due to loss of large ice masses and Arctic summer sea ice," *Nature Communications*, vol. 11, no. 1, p. 5177, 2020. [Online]. Available: https://doi.org/10.1038/s41467-020-18934-3

[3] Arctic Economic Council, "Arctic Connectivity Working Group 2021," 2021. [Online]. Available: https://arcticeconomiccouncil.com/wp-content/uploads/2021/05/aec-cwg-report-050721-6.pdf

[4] International Association of Lighthouse Authorities (IALA), "IALA GUIDELINE 1082 AN OVERVIEW OF AIS Edition 2.0," 2016.

[5] I. Varlamis, K. Tserpes, and C. Sardianos, "Detecting Search and Rescue Missions from AIS Data," in *2018 IEEE 34th International Conference on Data Engineering Workshops (ICDEW)*, 2018, pp. 60–65.

[6] D. Chen, Y. Zhao, P. Nelson, Y. Li, X. Wang, Y. Zhou, J. Lang, and X. Guo, "Estimating ship emissions based on AIS data for port of Tianjin, China," *Atmospheric Environment*, vol. 145, pp. 10–18, 2016. [Online]. Available: https://www.sciencedirect.com/science/article//S1352231016306926

[7] ITU-R, "Automatic identification system VHF data link loading," *Rep. ITU-R M.2287-0*, vol. 0, 2013.

[8] IALA, "VHF Data Exchange System (VDES)," *G1117*, no. December, pp. 1–20, 2017. [Online]. Available: https://www.iala-aism.org/product/vhd-data-exchange-system-vdes-overview-1117/

[9] T. Eriksen, L. Braten, A. N. Skauen, H. Haugli, L. Løge, A. Bjørnevik, F. Storesund, and N. Alagha, "VDE-SAT–Preliminary verification results for proposed satellite component of new maritime communication system," in *Proc. 4S Symp.*, 2018, pp. 1–14.

[10] F. Lázaro, R. Raulefs, W. Wang, F. Clazzer, and S. Plass, "VHF Data Exchange System (VDES): an enabling technology for maritime communications," *CEAS Space Journal*, vol. 11, no. 1, pp. 55–63, 2019. [Online]. Available: http://dx.doi.org/10.1007/s12567-018-0214-8

[11] N. Molina, F. Cabrera, V. Araña, and M. Tichavska, "An overview about the physical layer of the vhf data exchange system (vdes)," in *Computer Aided Systems Theory – EUROCAST 2019*, R. Moreno-Díaz, F. Pichler, and A. Quesada-Arencibia, Eds. Cham: Springer International Publishing, 2020, pp. 67–74.

[12] International Maritime Organization (IMO), "Guidance on the use of AIS Application-Specific Messages," 2010.

[13] R. I.-R. P.1546-6, "Method for point-to-area predictions for terrestrial services in the frequency range 30 MHz to 3 000 MHz P Series Radiowave propagation," 2009.

[14] I. J. Timmins and S. O'Young, "Marine communications channel modeling using the finite-difference time domain method," *IEEE Transactions on Vehicular Technology*, vol. 58, no. 6, pp. 2626–2637, 2009.

[15] C. Y. D. Sim, "The propagation of VHF and UHF radio waves over sea paths," Jan 2002. [Online]. Available: https://hdl.handle.net/2381/7444

[16] L. E. Bråten, V. Arneson, K. Svenes, T. Eriksen, and Ø. Olsen, "Channel Modelling for VHF Data Exchange System via Satellite," in *12th European Conference on Antennas and Propagation (EuCAP 2018)*. IET, 2018.

[17] H.-C. Haugli, L. Løge, N. Alagha, A. Bjørnevik, F. Storesund, S. Christiansen, T. Eriksen, and L. Bråten, "The VHF data exchange system (VDES) and Norsat-2 satellite testing," *35th AIAA International Communications Satellite Systems Conference, ICSSC 2017*, no. 204009, 2017.

[18] L. E. Bråten, T. Eriksen, A. N. Skauen, A. Bjernevik, H. C. Haugli, and L. Lege, "On the VHF radio channel for the data exchange system via satellite (VDE-SAT); experimental results from the NorSat-2 satellite experiment," in *36th International Communications Satellite Systems Conference (ICSSC 2018)*. IET, 2018, pp. 1–8.

[19] L. M. Bradbury, D. Diaconu, S. Molgat Laurin, A. M. Beattie, C. Ma, I. S. Spydevold, H. C. Haugli, R. E. Zee, J. Harr, and F. Udnæs, "NorSat-2: Enabling advanced maritime communication with VDES," *Acta Astronautica*, vol. 156, pp. 44–50, 2019. [Online]. Available: https://www.sciencedirect.com/science/article/pii/S0094576518303849

[20] G. Quintana-Diaz, T. Ekman, J. M. Lago Agra, D. Hurtado de Mendoza, A. González Muíño, and F. Aguado Agelet, "In-Orbit Measurements and Analysis of Radio Interference in the UHF Amateur Radio Band from the LUME-1 Satellite," *Remote Sensing*, vol. 13, no. 16, p. 3252, 2021.

BIOGRAPHY

Gara Quintana Díaz received her B.S. and M.Sc degrees in telecommunication engineering from University of Las Palmas (ULPGC). She is a Ph.D. Fellow at theNorwegian University of Science and Technology (NTNU) in the Department of Electronic Systems. Her research interests include in-orbit interference measurements from small satellites, software-defined radio platforms and satellite communication systems.

Roger Birkeland received his M.Sc. in Electronic Engineering at NTNU and is a post-doctoral researcher at NTNU in the Department of Electronic Systems. He received his Ph.D. in satellite communications in (2019) and is currently researching small satellite systems and heterogeneous communication systems for remote areas.

Lars Løge received a M.Sc. and a PhD in Electronics and Telecommunications from NTNU where he specialized in satellite communications. He worked 5 years as Adviser at the NOSA, studying solutions for satellite communications to the Arctic and liaison with related initiatives in Norway as well as internationally and through ESA, before starting at Space Norway AS in 2014 as Lead System Engineer in its subsidiary Statsat, which is in charge of operations, continuation and enhancement of the Norwegian AIS satellite constellation. In parallel he has supported the ESA funded VDE-SAT activities in Space Norway and since early 2015 he has been following the work in IALA and ITU on VDES and contributed to Recommendation ITU-R M.2092 as well as Report ITU-R M.2435. In preparation for and during WRC-19 he had the role as European Conference of Postal and Telecomunications Administrations (CEPT) Coordinator for WRC-19 Agenda Item 1.9.2 (VDE-SAT). Since December 2019 he has been VDES Program Manager at Space Norway.
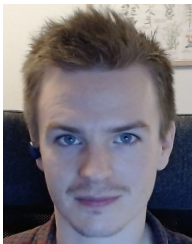
Even Andersen received a M.Sc. in physics from the University of Oslo and has worked at Space Norway AS as a software architect since 2018.

Anton Bolstad received a M.Sc. in Electronics Engineering from NTNU and has worked at Space Norway AS as a Systems Engineer since 2016.

Torbjörn Ekman received the M.Sc. degree in engineering physics in 1994 and the Ph.D. degree in signal processing in 2002, both from Uppsala University, Sweden. From 1997 to 1998 he was a visiting scientist at the Institute of Communications and Radio-Frequency Engineering, Vienna University of Technology, Vienna, Austria, on a Marie Curie Grant. From 1999 to 2002, he was visiting the Digital Signal Processing Group, University of Oslo, Norway. In 2002–2005, he made his postdoctoral studies at UniK, University Graduate Center, Kjeller, Norway. In 2006 he joined NTNU in Trondheim, Norway, where he is Professor at the Department of Electronic Systems. His current research interests include signal processing in wireless communications, micro satellite communication, Massive MIMO and dynamic radio channel modeling. He is currently participating in projects on micro satellites, autonomous ships, costal and arctic maritime operations and surveillance, radio resource management and channel modeling.

8